Robust layerwise C 0 finite element approach based on a variable separation method for the modeling of composite and sandwich plates

Philippe Vidal, Laurent Gallimard, Olivier Polit

Robust layerwise C^0 finite element approach based on a variable separation method for the modeling of composite and sandwich plates

P. Vidal *, L. Gallimard, O. Polit

LEME - UPL, Univ Paris Nanterre, 50 rue de Sèvres, 92410 Ville d'Avray, France

A B S T R A C T

This paper deals with a new approach using both the variable separation and a robust C^0 eight-node finite element for the modeling of composite plates. The displacement field is approximated as a sum of separated functions of the in-plane coordinates x, y and the transverse coordinate z. This choice yields to an iterative process that consists of solving a 2D and 1D problem successively at each iteration. In the thickness direction, a fourth-order expansion in each layer is considered. For the in-plane description, the main novelty consists in the formulation of a field compatible approximation for the transverse shear strain field, referred to as the CL8 interpolation. This latter has to be adapted to the particular framework of the separated representation. It allows us to eliminate the shear locking pathology by constraining only the z−constant transverse shear strain terms. Numerical assessments show the absence of locking problems as well as the enhanced robustness with respect to distorted element shapes in comparison to classical isoparametric approaches. This new CL8 plate element provides excellent convergence rates under different boundary and loading conditions, and it yields accurate displacements and stresses for both thick and thin composite and sandwich plates.

1. Introduction

The increasing use of composite laminates and sandwich structures in weight-sensitive industrial applications needs the development of appropriate robust design tools. While the 3D approach involves prohibitive computational cost, composite panels are conveniently modeled as two-dimensional plate/shell structures, based on geometric considerations. However, complicating effects, such as anisotropy, heterogeneity and transverse shear compliance, call for dedicated plate/shell models that overcome the limitation of the so-called classical models (Kirchhoff-Love (CLPT) or Reissner-Mindlin (FSDT)).

According to published research, it is nowadays well established that theoretical models for heterogeneous structures can be classified as Equivalent Single Layer approach (ESL) or Layer-Wise Models (LW) (see Ref. [1]). In the former model class, the number of unknowns is independent of the number of layers, contrary to the latter one where the number of unknowns increases with the number of constituting layers. In ESL models, the classical Love-Kirchhoff (CLT, [2]), and Reissner-Mindlin (FSDT, [3]) can be mentioned. The first one leads to inaccurate results for composites because both transverse and normal strains are neglected. The second one needs a shear correction factor. So, High-order Shear Deformation Theories (HSDT) are developed to enhance the kinematics with an at least parabolic transverse shear distribution ([4–6]) that may also exactly verify the stress boundary conditions at the top and bottom surfaces of the laminates (Third-order theory [7,8], sinus model [9]). Nevertheless, transverse shear and normal stress continuity conditions at the interfaces between layers are violated for these ESL models. Thus, LW models aim at overcoming these restrictions. We can mention the following contributions [5,8,10–17]. Note also the so-called variable kinematics models developed by Carrera and co-workers [18] through a dedicated Unified Formulation (CUF) which encompasses these approaches within a displacement-based or mixed formulation. As an alternative, another way to obtain new models is based on the introduction of interface conditions into higher-order models pertaining to the ESL or to the LW. This permits to reduce the number of unknowns and can be viewed as Zig-Zag models [19–22].

This above literature deals with only some aspects of the broad research activity about models for layered structures and corresponding finite element formulations. An extensive assessment of different approaches has been made in Refs. [23–27].

From the computational point of view, the development of robust Finite Elements (FE) is required to cope with the adopted two-dimensional plate/shell models, see, e.g., the discussion by Mac-

* Corresponding author.
E-mail address: philippe.vidal@parisnanterre.fr (P. Vidal).

Neal [28] about the FE technology employed for Kirchhoff-Love and Reissner-Mindlin shell models. In particular, a general, highly predictive plate FE should be free from numerical pathologies that could degrade the accuracy of the solution in case of distorted elements or extreme thickness ratios. The most characteristic example for this latter issue is transverse shear locking, a spurious over-constraint that dramatically underestimates the bending deformation of a thin, shear-deformable plate element. Several techniques have been devised to correct the transverse shear locking pathology affecting FSDT-based plate/shell elements, most of which can be stated from hybrid-mixed approaches [29]. The most widespread techniques are reduced integration methods, which, however, require a dedicated stabilization for preventing spurious zero-energy modes [30], or so-called B-bar methods [31], in which a specific constraint is used for the transverse shear strain field. Different approaches have been followed for constructing this modified strain field, such as Kirchhoff mode [32], Assumed Natural Strain (ANS) [33,34], Mixed Interpolation of Tensorial Components (MITC) [35], the field-consistency paradigm [36], Discrete Shear elements [37] or Discrete Shear Gap (DSG) [38].

Over the past years, the Proper Generalized Decomposition (PGD) has shown interesting features in the reduction model framework [39]. It has been used in the context of separation of coordinate variables in multi-dimensional PDEs [39]. In particular, it has been applied for composite plates in Ref. [40] based on a Navier-type solution and [41–43] using the FE method. The displacements are written under the form of a sum of products of bidimensional polynomials of (x, y) and unidimensional polynomials of z. Previous works have clearly proved that this approach could provide quasi-3D results for such structures, even for discriminating cases such as the consideration of the free-edge effects [44]. Moreover, the performance of the method is not affected by expensive computational costs occurring for LW models or 3D FEM approach. Nevertheless, all these previous works suffer from numerical pathologies, in particular the transverse shear locking. In the particular framework of the separated representation, note that the first alternative to overcome this drawback consists in the use of a selective integration as carried out in Ref. [45].

In this work, we propose to take advantage of the separated representation with higher-order expansion through the thickness to deduce an efficient and accurate approach for the modeling of composite plates without numerical pathologies. This study is focused on the determination of new interpolation functions for the in-plane functions. Hence, a special transverse shear locking correction is formulated by referring to the field consistency paradigm and applied only to the constant, thickness-independent part of the transverse shear strain, as the contribution of the higher-order terms vanish naturally for thin plates. For this, the method first proposed by Polit et al. [46] for FSDT, and subsequently extended to a refined kinematics [47,48], is here further extended to a high-order plate approach in conjunction with the PGD method.

We now outline the remainder of this article. First, the classical mechanical formulation is recalled. Then, the principles of the PGD are briefly given in the framework of our study. The particular assumption on the displacements yields a non-linear problem. An iterative process based on a fixed point strategy is performed to solve this one. Then, the new interpolation of the in-plane functions based on the field compatibility approach is built and it is shown how it is adapted to the separated representation with a higher-order z-expansion. The associated discretized problems to be solved are also given. Finally, numerical results are discussed to illustrate the performance of the method. A comprehensive investigation is proposed that concerns both the robustness of the method with respect to length-to-thickness ratio and mesh distortion, and the accuracy of the predicted displacements and stresses for homogeneous and composite plates. Sandwich structures under a localized pressure with a wide range of slenderness ratios are also considered.

2. Reference problem description: the governing equations

Let us consider a plate occupying the domain $\mathcal{V} = \Omega \times \Omega_z$ with $\Omega = [0,\ a] \times [0,\ b]$ $\Omega_z = [-h/2,\ h/2]$ in a Cartesian coordinate $(x,\ y,\ z)$. The plate is defined by an arbitrary region Ω in the $(x,\ y)$ plane, located at the midplane for $z = 0$, and by a constant thickness h. See Fig. 1.

2.1. Constitutive relation

The plate can be made of *NC* perfectly bonded orthotropic layers. Using matrix notation, the three dimensional constitutive law of the *kth* layer is given by:

$$\begin{bmatrix} \sigma_{11}^{(k)} \\ \sigma_{22}^{(k)} \\ \sigma_{33}^{(k)} \\ \sigma_{23}^{(k)} \\ \sigma_{13}^{(k)} \\ \sigma_{12}^{(k)} \end{bmatrix} = \begin{bmatrix} C_{11}^{(k)} & C_{12}^{(k)} & C_{13}^{(k)} & 0 & 0 & C_{16}^{(k)} \\ & C_{22}^{(k)} & C_{23}^{(k)} & 0 & 0 & C_{26}^{(k)} \\ & & C_{33}^{(k)} & 0 & 0 & C_{36}^{(k)} \\ & & & C_{44}^{(k)} & C_{45}^{(k)} & 0 \\ & sym & & & C_{55}^{(k)} & 0 \\ & & & & & C_{66}^{(k)} \end{bmatrix} \begin{bmatrix} \varepsilon_{11}^{(k)} \\ \varepsilon_{22}^{(k)} \\ \varepsilon_{33}^{(k)} \\ \gamma_{23}^{(k)} \\ \gamma_{13}^{(k)} \\ \gamma_{12}^{(k)} \end{bmatrix}$$

$$\text{i.e. } [\sigma^{(k)}] = [C^{(k)}]\ [\varepsilon^{(k)}] \tag{1}$$

where we denote the stress vector $[\sigma]$, the strain vector $[\varepsilon]$ and $C_{ij}^{(k)}$ the three-dimensional stiffness coefficients of the layer (k).

2.2. The weak form of the boundary value problem

Using the above matrix notation and for admissible displacement $\delta\vec{u} \in \delta U$, the variational principle is given by:

find $\vec{u} \in U$ (space of admissible displacements) such that

$$-\int_{\mathcal{V}} \left[\varepsilon(\delta\vec{u})\right]^T \left[\sigma(\vec{u})\right] d\mathcal{V} + \int_{\mathcal{V}} [\delta u]^T \left[b\right] d\mathcal{V} + \int_{\partial\mathcal{V}_F} [\delta u]^T [t]\, d\partial\mathcal{V} = 0,$$

$$\forall \delta\vec{u} \in \delta U \tag{2}$$

where $\left[b\right]$ and $[t]$ are the prescribed body and surface forces applied on $\partial\mathcal{V}_F$.

3. Application of the proper generalized decomposition method to plates

In this section, for sake of conciseness, we briefly introduce the application of the variable separation for the plate analysis that has been developed in Ref. [43].

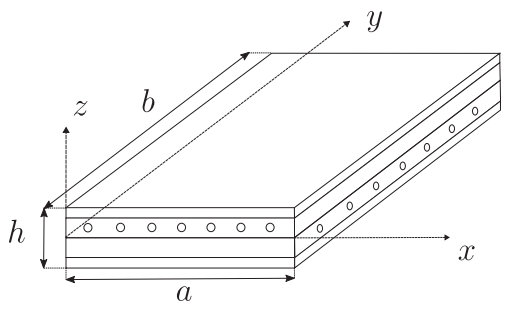

Fig. 1. Composite laminate and coordinate system.

3.1. The displacement and the strain field

The displacement solution $(u_1(x,y,z), u_2(x,y,z), u_3(x,y,z))$ is constructed as the sum of N products of functions of in-plane coordinates and transverse coordinate ($N \in \mathbb{N}$ is the order of the representation)

$$[u] = \begin{bmatrix} u_1(x,y,z) \\ u_2(x,y,z) \\ u_3(x,y,z) \end{bmatrix} = \sum_{i=1}^{N} \begin{bmatrix} f_1^i(z)\, v_1^i(x,y) \\ f_2^i(z)\, v_2^i(x,y) \\ f_3^i(z)\, v_3^i(x,y) \end{bmatrix} = \sum_{i=1}^{N} \begin{bmatrix} f_1^i(z) \\ f_2^i(z) \\ f_3^i(z) \end{bmatrix} \circ \begin{bmatrix} v_1^i(x,y) \\ v_2^i(x,y) \\ v_3^i(x,y) \end{bmatrix} \tag{3}$$

where (f_1^i, f_2^i, f_3^i) are defined in Ω_z and (v_1^i, v_2^i, v_3^i) are defined in Ω. The "$\circ$" operator is Hadamard's element-wise product.

In this paper, a classical eight-node FE approximation is used in Ω and a LW description is chosen in Ω_z as it is particularly suitable for the modeling of composite structure. The strain derived from Eq. (3) is

$$[\varepsilon(u)] = \begin{bmatrix} \varepsilon_{11} \\ \varepsilon_{22} \\ \varepsilon_{33} \\ \gamma_{23} \\ \gamma_{13} \\ \gamma_{12} \end{bmatrix} = \sum_{i=1}^{N} \begin{bmatrix} f_1^i\, v_{1,1}^i \\ f_2^i\, v_{2,2}^i \\ (f_3^i)'\, v_3^i \\ (f_2^i)'\, v_2^i + f_3^i\, v_{3,2}^i \\ (f_1^i)'\, v_1^i + f_3^i\, v_{3,1}^i \\ f_1^i\, v_{1,2}^i + f_2^i\, v_{2,1}^i \end{bmatrix} \tag{4}$$

where the prime stands for the classical derivative ($f_i' = \frac{df_i}{dz}$), and $(\,)_{,\alpha}$ for the partial derivative.

In order to introduce the transverse shear locking correction proposed in Section 4.3, the transverse shear strain field given in Eq. (4) is split into the classical z–constant contribution γ^0, and a contribution γ^h that depends on the thickness coordinate z and is related to high-order terms:

$$[\gamma(u)] = \begin{bmatrix} \gamma_{23} \\ \gamma_{13} \end{bmatrix} = \left[\gamma^0\right] + \left[\gamma^h\right] \tag{5}$$

where $[\gamma^0] = \begin{bmatrix} \gamma_{23}^0 \\ \gamma_{13}^0 \end{bmatrix}$ and $[\gamma^h] = \begin{bmatrix} \gamma_{23}^h \\ \gamma_{13}^h \end{bmatrix}$.

Thus, Eq. (4) can be written under the following form:

$$[\varepsilon(u)] = \sum_{i=1}^{N} \begin{bmatrix} 0 \\ 0 \\ 0 \\ [\gamma^0] = \begin{bmatrix} {}^0(f_2^i)'\, v_2^i + {}^0f_3^i\, v_{3,2}^i \\ {}^0(f_1^i)'\, v_1^i + {}^0f_3^i\, v_{3,1}^i \end{bmatrix} \\ 0 \end{bmatrix} + \begin{bmatrix} f_1^i\, v_{1,1}^i \\ f_2^i\, v_{2,2}^i \\ (f_3^i)'\, v_3^i \\ [\gamma^h] = \begin{bmatrix} {}^h(f_2^i)'\, v_2^i + {}^hf_3^i\, v_{3,2}^i \\ {}^h(f_1^i)'\, v_1^i + {}^hf_3^i\, v_{3,1}^i \end{bmatrix} \\ f_1^i\, v_{1,2}^i + f_2^i\, v_{2,1}^i \end{bmatrix} \tag{6}$$

where the following notation is retained: ${}^0g_j^i$ contains only the constant part of g_j^i while all z–dependency is contained in ${}^hg_j^i$. g stands for f' or f. So, we have $(f_j^i)' = {}^0(f_j^i)' + {}^h(f_j^i)'$ and $f_3^i = {}^0f_3^i + {}^hf_3^i$.

3.2. The problem to be solved

For sake of clarity, the surface forces are neglected in the developments and the weak form of the plate problem introduced in Eq. (2) simplifies in

$$a(\vec{u}, \delta\vec{u}) = b(\delta\vec{u})$$

$$\text{with} \quad \begin{cases} a(\vec{u}, \delta\vec{u}) = \displaystyle\int_\Omega \int_{\Omega_z} \left([\varepsilon(\delta\vec{u})]^T [C] [\varepsilon(\vec{u})] \right) dz\, d\Omega \\ b(\delta\vec{u}) = \displaystyle\int_\Omega \int_{\Omega_z} [\delta u]^T [b]\, dz\, d\Omega \end{cases} \tag{7}$$

where $[C]$ represents, in each layer (k), the matrix of the elastic moduli.

Eq. (7) is solved by an iterative procedure. If we assume that the first n functions have been already computed, the trial function for the iteration $n+1$ is written as

$$\left[u^{n+1}\right] = \left[u^n\right] + \begin{bmatrix} f_1 v_1 \\ f_2 v_2 \\ f_3 v_3 \end{bmatrix} = \left[u^n\right] + [f] \circ [v] \tag{8}$$

where (v_1, v_2, v_3), (f_1, f_2, f_3) are the functions to be computed and $\left[u^n\right]$ is the associated known set at iteration n defined by

$$\left[u^n\right] = \sum_{i=1}^{n} \begin{bmatrix} f_1^i v_1^i \\ f_2^i v_2^i \\ f_3^i v_3^i \end{bmatrix} \tag{9}$$

The test function is

$$\delta \begin{bmatrix} f_1 v_1 \\ f_2 v_2 \\ f_3 v_3 \end{bmatrix} = \begin{bmatrix} \delta f_1 v_1 + f_1 \delta v_1 \\ \delta f_2 v_2 + f_2 \delta v_2 \\ \delta f_3 v_3 + f_3 \delta v_3 \end{bmatrix} = [\delta f] \circ [v] + [\delta v] \circ [f] \tag{10}$$

with

$$[v] = \begin{bmatrix} v_1 \\ v_2 \\ v_3 \end{bmatrix} \quad [f] = \begin{bmatrix} f_1 \\ f_2 \\ f_3 \end{bmatrix} \tag{11}$$

The test function defined by Eq. (10) and the trial function defined by Eq. (8) are introduced into the weak form Eq. (7) to obtain the two following equations:

$$a(f \circ v, f \circ \delta v) = b(f \circ \delta v) - a(u^n, f \circ \delta v) \tag{12}$$

$$a(v \circ f, v \circ \delta f) = b(v \circ \delta f) - a(u^n, v \circ \delta f) \tag{13}$$

As these equations define a coupled non linear problem, a non linear resolution strategy has to be used. Classically, a fixed point method is carried out. An initial function $f^{(0)}$ is set, and at each step, the algorithm computes a new pair $(v^{(m+1)}, f^{(m+1)})$ such that

- $v^{(m+1)}$ satifies Eq. (12) for f set to $f^{(m)}$ (linear resolution on Ω)
- $f^{(m+1)}$ satifies Eq. (13) for v set to $v^{(m+1)}$ (linear resolution on Ω_z)

The fixed point algorithm is stopped when

$$\frac{\|v^{(m+1)} \circ f^{(m+1)} - v^{(m)} \circ f^{(m)}\|_{\mathcal{V}}}{\|v^{(0)} \circ f^{(0)}\|_{\mathcal{V}}} \leq \epsilon \tag{14}$$

where $\|A\|_{\mathcal{V}} = \left[\int_\Omega \int_{\Omega_z} \sum_{i=1}^{3} A_i^2 \, dx\, dy\, dz \right]^{1/2}$ and ϵ is a small parameter to be fixed by the user.

4. Description of the new finite element approximations for the transverse shear strains

Based on the weak form introduced in Eq. (12) and Eq. (13), a discrete representation of the functions (v, f) must be introduced. This section is only dedicated to the finite element approximations of the geometry Ω and the generalized associated displacements v, defined in the previous section. For this purpose, an eight-node quadrilateral FE approximation is considered and associated with the new CL8 approximation for avoiding transverse shear locking problems and minimizing the convergence rate loss for distorted meshes.

Note that the approximation of f will be given in Section 5.

4.1. The geometric approximation

The eight-node quadrilateral finite element is presented in Fig. 2. The in-plane coordinates (x, y) are approximated on the reference bi-unit domain with respect to the reduced coordinates (ξ, η) by:

$$\begin{cases} x(\xi,\eta) = \sum_{i=1}^{8} Nq_i(\xi,\eta)(x)_i \\ y(\xi,\eta) = \sum_{i=1}^{8} Nq_i(\xi,\eta)(y)_i \end{cases} \tag{15}$$

where $Nq_i(\xi, \eta)$ are the classical Serendipity interpolation functions, see Appendix A.

4.2. Isoparametric interpolation

An isoparametric procedure is used and unknown functions $v_i(x, y)$ are approximated using the same functions as the geometry, see Eq. (15). The elementary vector of degrees of freedom (dof) associated with one element Ω_e of the mesh in Ω is denoted $[q_e^v]$. The displacement fields and the strain fields are determined from the values of $[q_e^v]$ by

$$[v_e] = [N_{xy}][q_e^v], \quad [\mathcal{E}_v^e] = [B_{xy}][q_e^v] \tag{16}$$

where

$$[\mathcal{E}_v^e]^T = \begin{bmatrix} v_1 & v_{1,1} & v_{1,2} & v_2 & v_{2,1} & v_{2,2} & v_3 & v_{3,1} & v_{3,2} \end{bmatrix}$$

The matrices $[N_{xy}]$ and $[B_{xy}]$ contain the interpolation functions, their derivatives and the jacobian components.

4.3. The CL8 interpolation

The isoparametric interpolation for the transverse shear strains leads to a locking phenomenon because of the incompatibility of the polynomial spaces defined by the sum of v_α^i and the in-plane derivative $v_{3,\alpha}$ (α = 1, 2 for γ_{13}^0 and γ_{23}^0, respectively) [47]. The locking pathology is associated to the z–constant part only, for higher-order contributions depend on the plate thickness and vanish naturally in the thin plate limit. Thus, a field-compatible interpolation for the eight-node element is constructed for the z–constant part γ^0 as it has been previously developed in Ref. [49] for FSDT plate elements, in Ref. [47] to a refined plate element and in Ref. [48] in the framework of the Carrera's Unified Formulation (CUF). It is recalled briefly hereafter. Then, this deduced new interpolation is extended in the particular framework of the separated representation where no rotation dof appears in the kinematics.

The so-called "field compatibility" approach is based on the following steps:

- In order to enhance the robustness of the element for distorted shapes, the z–constant part of transverse shear strain components γ^0 is first written in the reduced coordinates (ξ, η).
- In order to ensure the same polynomial approximation for the in-plane functions (v_ξ, v_η) and the derivatives of the transverse displacement, v_3 is assumed to be cubic, introducing four supplementary dofs at the mid-side nodes.
- A linear variation of the tangential transverse shear strain component is assumed on each side of the elementary domain, see Fig. 2. Thus, the supplementary dof introduced at the previous step can be expressed as a linear combination of the v_ξ, v_η and transverse displacement u_3 dof. Therefore, a new finite element approximation is obtained for the transverse displacement v_3. The resulting eight-node FE will be denoted CL8 due to the Cubic and Linear approximations employed for the transverse deflection and the tangential transverse shear strain, respectively.
- The interpolation of the reduced transverse shear strain components is defined in the following polynomial basis as the intersection sets of monomial terms from ξ and η:

$$\begin{aligned} \mathcal{B}(\gamma_\xi^0) &= \mathcal{B}(v_\xi) \cap \mathcal{B}(v_{3,\xi}) = \{1, \xi, \eta, \xi\,\eta, \eta^2\} \\ \mathcal{B}(\gamma_\eta^0) &= \mathcal{B}(v_\eta) \cap \mathcal{B}(v_{3,\eta}) = \{1, \xi, \eta, \xi\,\eta, \xi^2\} \end{aligned} \tag{17}$$

- According to the dimension of the polynomial basis, five points are needed for each reduced transverse shear strains. These points were choosen as indicated in Fig. 3 because this location gives the best results in case of distorted meshes, see Refs. [49,50]. The following finite element approximation is obtained for the reduced transverse shear strains:

$$\gamma_\xi^0(\xi,\eta) = \sum_{I=1}^{5} C\xi_I(\xi,\eta)\gamma_{\xi I}^0 \quad \gamma_\eta^0(\xi,\eta) = \sum_{J=1}^{5} C\eta_J(\xi,\eta)\gamma_{\eta J}^0 \tag{18}$$

  where $C\xi_I$ and $C\eta_J$ are interpolation functions, see Ref. [46].
- Using the jacobian matrix, the physical transverse shear strains γ_{23}^0 and γ_{13}^0 are deduced from the reduced transverse shear strains of Eq. (18).

$$\begin{bmatrix} \gamma_{23}^0(\xi,\eta) \\ \gamma_{13}^0(\xi,\eta) \end{bmatrix} = [J]^{-1} \begin{bmatrix} \gamma_\eta^0(\xi,\eta) \\ \gamma_\xi^0(\xi,\eta) \end{bmatrix} \tag{19}$$

From this field compatibility approach, a new interpolation of v_1^i, v_2^i, and v_3^i based on Eq. (19) is deduced for the constant part of the transverse shear strain (denoted γ^0 in Eq. (4)). Thus, for our particular separated representation, it can be expressed under the two following forms depending of the problem to be solved:

$$\begin{cases} [\gamma^0(f \circ v)] = \begin{bmatrix} \gamma_{23}^0(\xi,\eta) \\ \gamma_{13}^0(\xi,\eta) \end{bmatrix} = [\Sigma_{zgam}(f)][\mathcal{E}_{v_{CL8}}] \\ \text{or} \\ [\gamma^0(v \circ f)] = [\Sigma_{xy_{CL8}}(v)][\mathcal{E}_{0_f}] \end{cases} \tag{20}$$

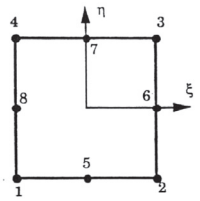

Fig. 2. The reference domain of the 8-node finite element.

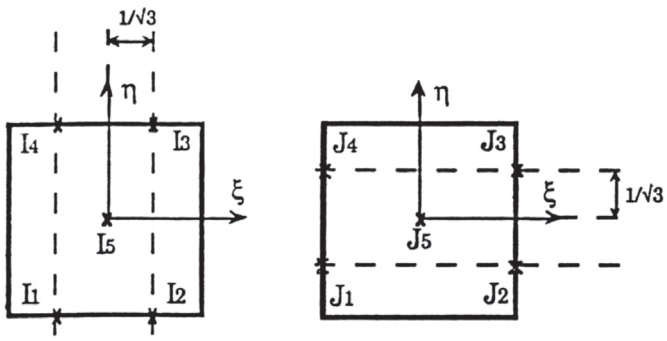

Fig. 3. Point locations for the transverse shear strains evaluations.

where

$$[\Sigma_{zgam}(f)] = \begin{bmatrix} 0 & 0 & 0 & {}^0(f_2)' & 0 & 0 & 0 & 0 & {}^0f_3 \\ {}^0(f_1)' & 0 & 0 & 0 & 0 & 0 & 0 & {}^0f_3 & 0 \end{bmatrix}$$

$$[\Sigma_{xy_{CL8}}(v)] = \begin{bmatrix} 0 & 0 & 0 & v_2 & v_{3,2} & 0 \\ 0 & v_1 & 0 & 0 & v_{3,2} & 0 \end{bmatrix}_{CL8}$$

and

$$[\mathcal{E}_{v_{CL8}}] = [B_{xy}^{CL8}][q_e^v] \tag{21}$$

$$[\mathcal{E}_{0_f}] = \begin{bmatrix} {}^0f_1 & {}^0f_1' & {}^0f_2 & {}^0f_2' & {}^0f_3 & {}^0f_3' \end{bmatrix}$$

$[B_{xy}^{CL8}]$ contains the new interpolation functions defined previously, it depends on $C\xi_I$ and $C\eta_J$. The subscript $_{CL8}$ recalls that the involved function v is calculated with the new CL8 interpolation functions. It is not detailed here for brevity reason, but it can be found in Ref. [46].

5. Finite element discretization

The new discrete representation of the functions v is defined in Section 4.3. As far as the function f is concerned, a fourth-order FE expansion is chosen as it is particularly suitable for the modeling of composite structures. The elementary vector of dofs associated with one element Ω_{z_e} of the mesh in Ω_z is denoted $[q_e^f]$. The displacement fields f_e and the two parts of the strain fields $[\mathcal{E}_{0_f}]$, $[\mathcal{E}_{h_f}]$ associated to $[\gamma^0]$ and $[\gamma^h]$ respectively, are determined from the values of $[q_e^f]$ by

$$[f_e] = [N_z][q_e^f] \quad \text{and} \quad [\mathcal{E}_{h_f}] = [B_z^h][q_e^f], \quad [\mathcal{E}_{0_f}] = [B_z^0][q_e^f] \tag{22}$$

where

- $[\mathcal{E}_{h_f}]^T = \begin{bmatrix} f_1 & {}^hf_1' & f_2 & {}^hf_2' & {}^hf_3 & f_3' \end{bmatrix}$
- $[\mathcal{E}_{0_f}]$ is defined in Eq. (21).

The matrices $[N_z]$, $[B_z^0]$, $[B_z^h]$ contain the 1D interpolation functions, their derivatives and the jacobian components. Note that the constant part of $f_1'(z)$, $f_2'(z)$ and $f_3(z)$ are included in $[\mathcal{E}_{0_f}]$, while the high-order terms are in $[\mathcal{E}_{h_f}]$.

In the two following sections, these FE representations and those described in Section 4 are introduced in Eq. (12) and Eq. (13) to deduce the alternative linear problems to be solved.

5.1. Finite element problem to be solved on Ω

For the sake of simplicity, the function $f^{(m)}$ which is assumed to be known, will be denoted $\widetilde{f}$, and the function $v^{(m+1)}$ to be computed will be denoted v.

Using Eq. (20), the strain, split into 2 terms in Eq. (4), can be expressed in matrix notations as

$$[\varepsilon(\widetilde{f} \circ v)] = [\Pi_{\gamma^0}][\Sigma_{zgam}(\widetilde{f})][\mathcal{E}_{v_{CL8}}] + [\Sigma_z(\widetilde{f})][\mathcal{E}_v] \tag{23}$$

with

$$[\Pi_{\gamma^0}] = \begin{bmatrix} 0 & 0 \\ 0 & 0 \\ 0 & 0 \\ 1 & 0 \\ 0 & 1 \\ 0 & 0 \end{bmatrix}$$

$$[\Sigma_z(\widetilde{f})] = \begin{bmatrix} 0 & \widetilde{f}_1 & 0 & 0 & 0 & 0 & 0 & 0 & 0 \\ 0 & 0 & 0 & 0 & 0 & \widetilde{f}_2 & 0 & 0 & 0 \\ 0 & 0 & 0 & 0 & 0 & 0 & \widetilde{f}_3' & 0 & 0 \\ 0 & 0 & 0 & {}^h\widetilde{f}_2' & 0 & 0 & 0 & 0 & {}^h\widetilde{f}_3' \\ {}^h\widetilde{f}_1' & 0 & 0 & 0 & 0 & 0 & 0 & {}^h\widetilde{f}_3 & 0 \\ 0 & 0 & \widetilde{f}_1 & 0 & \widetilde{f}_2 & 0 & 0 & 0 & 0 \end{bmatrix} \tag{24}$$

This expression allows us to separate the dependance with respect to the functions f and v. It can be introduced in Eq. (12) to deduce the problem on Ω with separated integrations on Ω and Ω_z. Thus, we deduce:

$$\begin{aligned} a(\widetilde{f} \circ v, \widetilde{f} \circ \delta v) = \int_\Omega & [\delta\mathcal{E}_v]^T[k_z(\widetilde{f})][\mathcal{E}_v] + [\delta\mathcal{E}_v]^T[k_{zvv_{CL8}}(\widetilde{f})][\mathcal{E}_{v_{CL8}}] \\ & + [\delta\mathcal{E}_{v_{CL8}}]^T[k_{zv_{CL8}v}(\widetilde{f})][\mathcal{E}_v] \\ & + [\delta\mathcal{E}_{v_{CL8}}]^T[k_{zv_{CL8}v_{CL8}}(\widetilde{f})][\mathcal{E}_{v_{CL8}}]d\Omega \end{aligned} \tag{25}$$

with

$$\begin{aligned} [k_z(\widetilde{f})] &= \int_{\Omega_z} [\Sigma_z(\widetilde{f})]^T[C][\Sigma_z(\widetilde{f})]dz \\ [k_{zvv_{CL8}}(\widetilde{f})] &= \int_{\Omega_z} [\Sigma_z(\widetilde{f})]^T[C][\Pi_{\gamma^0}][\Sigma_{zgam}(\widetilde{f})]dz \\ [k_{zv_{CL8}v}(\widetilde{f})] &= [k_{zvv_{CL8}}(\widetilde{f})]^T \\ [k_{zv_{CL8}v_{CL8}}(\widetilde{f})] &= \int_{\Omega_z} [\Sigma_{zgam}(\widetilde{f})]^T[\Pi_{\gamma^0}]^T[C][\Pi_{\gamma^0}][\Sigma_{zgam}(\widetilde{f})]dz \end{aligned} \tag{26}$$

and

$$\begin{aligned} b(\widetilde{f} \circ \delta v) = & \int_\Omega [\delta v]^T[b_z(\widetilde{f})]d\Omega - \int_\Omega \Big([\delta\mathcal{E}_v]^T[\sigma_z(\widetilde{f}, u^n)] \\ & + [\delta\mathcal{E}_{v_{CL8}}]^T[\sigma_{z_{CL8}}(\widetilde{f}, u^n)] \Big) d\Omega \end{aligned} \tag{27}$$

with

$$[b_z(\widetilde{f})] = \int_{\Omega_z} \left[\widetilde{f}\right] \circ [b]dz \tag{28}$$

$$[\sigma_z(\widetilde{f}, u^n)] = \int_{\Omega_z} [\Sigma_z(\widetilde{f})]^T[C][\varepsilon(u^n)]dz \tag{29}$$

$$[\sigma_{z_{CL8}}(\widetilde{f}, u^n)] = \int_{\Omega_z} [\Sigma_{zgam}(\widetilde{f})]^T[\Pi_{\gamma^0}]^T[C][\varepsilon(u^n)]dz \tag{30}$$

The introduction of the finite element approximation Eq. (16) and the new CL8 interpolation Eq. (21) in Eq. (25) and Eq. (27) of the variational Eq. (12) leads to the linear system

$$\left[K_z(\widetilde{f})\right][q^v] = \left[\mathcal{R}_v(\widetilde{f}, u^n)\right] \tag{31}$$

where

- $[q^v]$ is the vector of the nodal displacements associated with the finite element mesh in Ω,
- $\left[K_z(\widetilde{f})\right]$ is the stiffness matrix obtained by summing the elements' stiffness matrices

$$\begin{aligned} \left[K_z^e(\widetilde{f})\right] = \int_{\Omega_e} & [B_{xy}]^T[k_z(\widetilde{f})][B_{xy}] + [B_{xy}]^T[k_{zvv_{CL8}}(\widetilde{f})][B_{xy}^{CL8}] \\ & + [B_{xy}^{CL8}]^T[k_{zv_{CL8}v}(\widetilde{f})][B_{xy}] \\ & + [B_{xy}^{CL8}]^T[k_{zv_{CL8}v_{CL8}}(\widetilde{f})][B_{xy}^{CL8}]d\Omega_e \end{aligned}$$

- $\left[\mathcal{R}_v(\widetilde{f}, u^n)\right]$ is the equilibrium residual obtained by summing the elements' residual load vectors

$$\left[\mathcal{R}_v^e(\widetilde{f},u^n)\right]=\int_{\Omega_e}[N_{xy}]^T[b_z(\widetilde{f})]d\Omega_e-\int_{\Omega_e}[B_{xy}]^T[\sigma_z(\widetilde{f},u^n)]+[B_{xy}^{CL8}]^T[\sigma_{z_{CL8}}(\widetilde{f},u^n)]\,d\Omega_e$$

5.2. Finite element problem to be solved on Ω_z

For the sake of simplicity, the function $v^{(m+1)}$ which is assumed to be known, will be denoted $\widetilde{v}$, and the function $f^{(m+1)}$ to be computed will be denoted f. As previously, the strain defined in Eq. (4) is written in matrix notations as

$$[\varepsilon(\widetilde{v}\circ f)]=[\Pi_{\gamma^0}][\Sigma_{xy_{CL8}}(\widetilde{v})][\mathcal{E}_{0_f}]+[\Sigma_{xy}(\widetilde{v})][\mathcal{E}_{h_f}] \tag{32}$$

with

$$[\Sigma_{xy}(\widetilde{v})]=\begin{bmatrix}\widetilde{v}_{1,1}&0&0&0&0&0\\0&0&\widetilde{v}_{2,2}&0&0&0\\0&0&0&0&0&\widetilde{v}_3\\0&0&0&\widetilde{v}_2&\widetilde{v}_{3,2}&0\\0&\widetilde{v}_1&0&0&\widetilde{v}_{3,1}&0\\\widetilde{v}_{1,2}&0&\widetilde{v}_{2,1}&0&0&0\end{bmatrix} \tag{33}$$

$$[\Sigma_{xy_{CL8}}(\widetilde{v})]=\begin{bmatrix}0&0&0&\widetilde{v}_2&\widetilde{v}_{3,2}&0\\0&\widetilde{v}_1&0&0&\widetilde{v}_{3,1}&0\end{bmatrix}_{CL8} \tag{34}$$

Note that this expression ensures the separation of the constant part of γ^0 and the higher-order ones. It can be introduced in Eq. (13) to deduce the problem on Ω_z with separated integrations on Ω and Ω_z. Thus, we deduce:

$$a(\widetilde{v}\circ f,\widetilde{v}\circ\delta f)=\int_{\Omega_z}[\delta\mathcal{E}_{h_f}]^T[k_{xy}(\widetilde{v})][\mathcal{E}_{h_f}]+[\delta\mathcal{E}_{0_f}]^T[k_{xy^0f^hf}(\widetilde{v})][\mathcal{E}_{h_f}]+[\delta\mathcal{E}_{h_f}]^T[k_{xy^hf^0f}(\widetilde{v})][\mathcal{E}_{0_f}]+[\delta\mathcal{E}_{0_f}]^T[k_{xy^0f^0f}(\widetilde{v})][\mathcal{E}_{0_f}]dz \tag{35}$$

with

$$\begin{aligned}[k_{xy}(\widetilde{v})]&=\int_\Omega[\Sigma_{xy}(\widetilde{v})]^T[C][\Sigma_{xy}(\widetilde{v})]d\Omega\\[k_{xy^0f^hf}(\widetilde{v})]&=\int_\Omega[\Sigma_{xy_{CL8}}(\widetilde{v})]^T[\Pi_{\gamma^0}]^T[C][\Sigma_{xy}(\widetilde{v})]d\Omega\\[k_{xy^hf^0f}(\widetilde{v})]&=[k_{xy^0f^hf}(\widetilde{v})]^T\\[k_{xy^0f^0f}(\widetilde{v})]&=\int_\Omega[\Sigma_{xy_{CL8}}(\widetilde{v})]^T[\Pi_{\gamma^0}]^T[C][\Pi_{\gamma^0}][\Sigma_{xy_{CL8}}(\widetilde{v})]d\Omega\end{aligned} \tag{36}$$

and

$$b(\widetilde{v}\circ\delta f)=\int_{\Omega_z}[\delta f]^T[b_{xy}(\widetilde{v})]\,dz-\int_{\Omega_z}\left([\delta\mathcal{E}_{h_f}]^T[\sigma_{xy^hf}(\widetilde{v},u^n)]+[\delta\mathcal{E}_{0_f}]^T[\sigma_{xy^0f}(\widetilde{v},u^n)]\right)dz \tag{37}$$

with

$$[b_{xy}(\widetilde{v})]=\int_\Omega\left[\widetilde{v}\right]\circ[b]d\Omega \tag{38}$$

$$\begin{aligned}[\sigma_{xy^hf}(\widetilde{v},u^n)]&=\int_\Omega[\Sigma_{xy}(\widetilde{v})]^T[C][\varepsilon(u^n)]d\Omega\\[\sigma_{xy^0f}(\widetilde{v},u^n)]&=\int_\Omega[\Sigma_{xy_{CL8}}(\widetilde{v})]^T[\Pi_{\gamma^0}]^T[C][\varepsilon(u^n)]\,d\Omega\end{aligned} \tag{39}$$

The introduction of the finite element approximation Eq. (22) in Eq. (35) and Eq. (37) of the variational Eq. (13) leads to the linear system

$$\left[K_{xy}(\widetilde{v})\right]\left[q^f\right]=\left[\mathcal{R}_f(\widetilde{v},u^n)\right] \tag{40}$$

where

- $\left[q^f\right]$ is the vector of the nodal displacements associated with the finite element mesh in Ω_z,
- $\left[K_{xy}(\widetilde{v})\right]$ is the stiffness matrix obtained by summing the elements' stiffness matrices

$$\left[K_{xy}^e(\widetilde{v})\right]=\int_{\Omega_{z_e}}[B_z^h]^T[k_{xy}(\widetilde{v})][B_z^h]+[B_z^0]^T[k_{xy^0f^hf}(\widetilde{v})][B_z^h]+[B_z^h]^T[k_{xy^hf^0f}(\widetilde{v})][B_z^0]+[B_z^0]^T[k_{xy^0f^0f}(\widetilde{v})][B_z^0]dz_e$$

- $\left[\mathcal{R}_f(\widetilde{v},u^n)\right]$ is the equilibrium residual obtained by summing the elements' residual load vectors

$$\left[\mathcal{R}_f^e(\widetilde{v},u^n)\right]=\int_{\Omega_{z_e}}[N_z]^T[b_{xy}(\widetilde{v})]dz_e-\int_{\Omega_{z_e}}\left([B_z^h]^T[\sigma_{xy^hf}(\widetilde{v},u^n)]+[B_z^0]^T[\sigma_{xy^0f}(\widetilde{v},u^n)]\right)dz_e$$

6. Numerical results

In this section, several numerical benchmark tests available in open literature are presented in order to evaluate the accuracy and robustness of this new F.E approach in the framework of a separated representation. A first set of problems involving a simple homogeneous and isotropic plate is considered to assess the performance of the approach, i.e., the convergence rate for thin and thick plates, and the sensitivity with respect to distorted element shapes; these latter tests are conducted on a square plate with distorted mesh and a circular plate. Then, laminated composite and sandwich plates are analyzed to show the accuracy of both displacements and stresses. Global and localized pressures are used to show the performance of the separated variable in conjunction with the new CL8 interpolation functions.

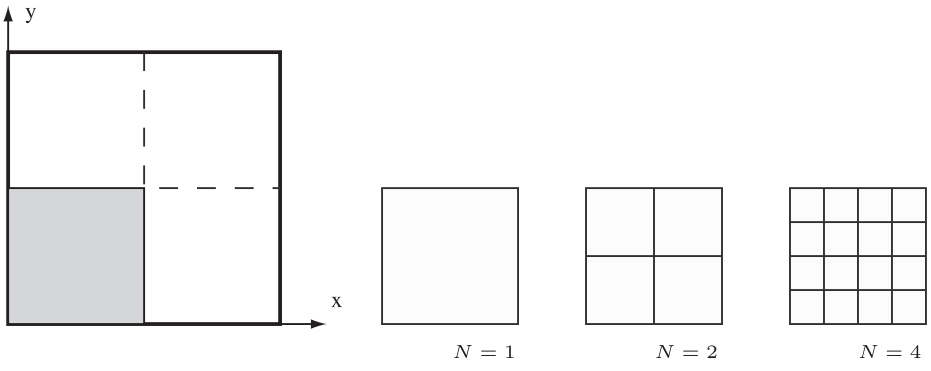

Fig. 4. Regular meshes for a quarter of the plate.

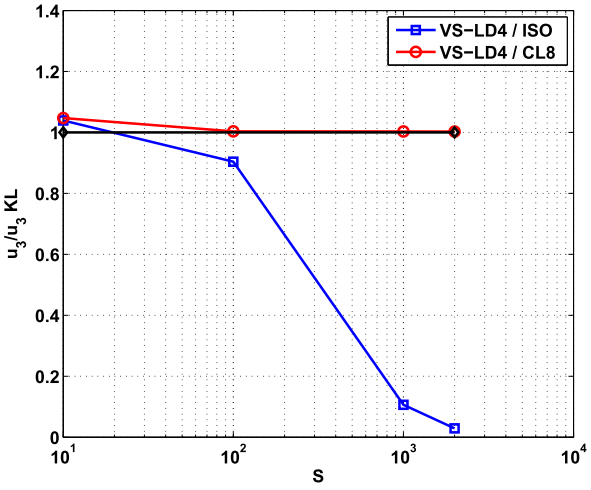

Fig. 5. Transverse displacement with respect to slenderness ratio S.

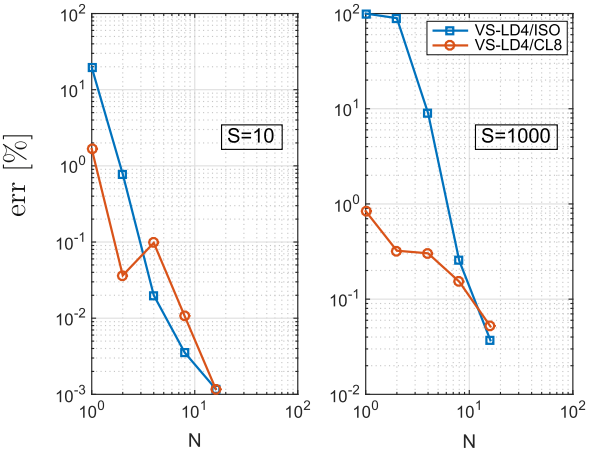

Fig. 6. Convergence of the transverse displacement for two length-to-thickness ratios.

In this section, two approaches based on the separated representation with a fourth-order expansion in the thickness direction are assessed:

VS-LD4/ISO: full-integrated isoparametric element (3×3 Gauss points for the whole stiffness matrix)
VS-LD4/CL8: CL8 approximation

Note that only one element per layer is used in the subsequent test cases.

6.1. *The transverse shear locking phenomenon*

The sensitivity to the transverse shear locking must be evaluated using the same mesh for different length to thickness ratios. The locking occurs if this ratio influences the convergence velocity: more the plate is thin, more the convergence velocity is slow and refined mesh must be used to reach the asymptotic value.

Therefore, the following test is considered:

geometry: square plate $a \times a$ and thickness $e = 10^{-n}$ with $n \in \{0, 4\}$
boundary conditions: simply supported on all sides, uniform transverse load p_0
materials: isotropic material with $E = 10.92$ and $\nu = 0.3$
mesh: regular mesh with $N = 2, 4, 8, 16$ (see Fig. 4)
results: the transverse displacement at the center of the plate for $z = 0$,

reference value is obtained by Kirchhoff-Love theory ($D = \frac{E}{12(1-\nu^2)}$).

$$U_3^a(a/2, a/2, 0) = 0.00406 \; p_0 \; \frac{a^4}{h^3 \; D}$$

For this test case, two couples are built to recover the solution, even if only one couple is sufficient to obtain the displacement value with accuracy. To assess the sensitivity to the transverse shear locking of the present approach, the results are shown in two different ways:

- *Constant mesh, varying slenderness ratio*

A coarse regular mesh with $N = 2$ elements is considered for the quarter plate (see Fig. 4) and the results are given for varying length-to-thickness ratios $S = a/h$. It can be inferred from Fig. 5 that the full-integrated isoparametric element suffers a very strong locking as the plate becomes thin ($S \geq 10^2$). On the contrary, the CL8 element is free from transverse shear locking and provide the reference Kirchhoff-Love values with good accuracy. The discrepancy for $S \leq 10^2$ in Fig. 5 between present F.E and the Kirchhoff-Love solution is due to the inadequation of this model in the semi-thick to thick range.

- *Convergence analysis for a thin or thick plate*

The convergence curves of the transverse displacement at the plate's center with respect to the mesh density are shown in log-log scale in Fig. 6 for various length-to-thickness ratios ($S = 10, 10^3$). The 3D elasticity solution is chosen as a reference one for $S = 10$. The previous comments are confirmed: the convergence rate of the full-integrated

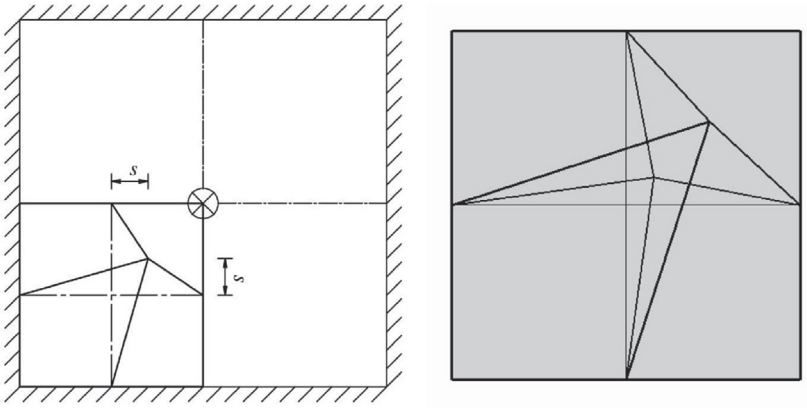

Fig. 7. Clamped square plate used for mesh sensitivity and meshes for $s = 0, 4, 12$.

ISO element is shown to strongly degrade as the length-to-thickness ratio S increases, a behavior that clearly indicates the presence of the transverse shear locking pathology. For a thick plate ($S = 10$), the CL8 methodology improves the accuracy for coarse meshes. For a thinner mesh, the error rate becomes very small and are also due to rounding error. Note that the strictly non-monotone convergence of the CL8 approach is due to the separated unknowns method. Despite this feature, the performance of the present approach is slightly improved by the proposed correction.

6.2. The distorsion tests

In this section, the sensitivity of the present FE approach to the mesh distortion is illustrated on two test cases widely used in open literature, namely the square and circular plate.

6.2.1. Square isotropic plate test

This test, see Fig. 7, is often used to investigate the mesh sensitivity in plate bending problems [51]. The following datas are considered:

geometry: square plate of length $a = 100$ and thickness $h = 1$;
boundary conditions: clamped and submitted to a concentrated load at the center $F_3 = 178.5714$;
materials: isotropic material with $E = 10.92\ 10^4$ and $\nu = 0.3$
mesh: $N = 2$ for the quarter of the plate, using the parameter $s \in \{0, 4, 8, 12\}$ defining the distorsion of the mesh,
result: displacements U_3 at the center for $z = 0$,
reference values: Kirchhoff-Love solution, given by $U_3 = 0.0056 \quad F_3 \frac{L^2}{h^3 D} = 1$ with $D = \frac{E}{12(1-\nu^2)}$.

In this test, the distorted meshes are characterized by the parameter s defining the coordinates of the mid-node of the quarter plate $(a/4 + s, a/4 + s)$. Note that an undistorted mesh corresponds to $(s = 0)$, i.e. $x_1 = x_2 = a/4$. Two distorded meshes ($s = 4$, 12) and the regular mesh ($s = 0$) are presented in Fig. 7 and the most distorted one is obtained for $s = 12$. For this mesh, the coordinates of the center node are (37, 37) while the middle point coordinates of the straight line connecting the two corner nodes are (37.5, 37.5). It is the most distorded mesh which can be built. The transverse displacement is presented in Table 1. 5 couples are built. For the regular mesh, a discrepancy of 2.5% is obtained for the maximum deflection while the error is always less than 10% for all the distorted meshes. This CL8 F.E. is very robust with respect to distorsion sensitivity on this test and the accuracy is significantly improved with respect to the ISO approach. In fact, this latter induces an error rate of more than 80% regardless of the distorsion level.

6.2.2. Circular isotropic plate

This test is also presented in order to evaluate the sensitivity to mesh distorsion and the effect of different boundary conditions. The following data are considered:

geometry: circular plate with radius $R = 5$, two thicknesses $h = 1.$ and 0.1;
boundary conditions: simply supported (SA-2) avoiding only transverse displacement, and clamped (ENC); uniform transverse load of 10^{-4}
materials: isotropic material with $E = 1.7472\ 10^7$ and $\nu = 0.3$
mesh: $N = 1$; 3; 12; 28 for the quarter of the circular plate, see Fig. 8
result and location: displacements U_3 at the center,
reference values are the Kirchhoff-Love solutions.

Table 1
Clamped square plate results.

s	0.	4.	8.	12.
U_3 VS-LD4/CL8	0.975	0.940	0.922	0.900
U_3 VS-LD4/ISO	0.224	0.197	0.152	0.109

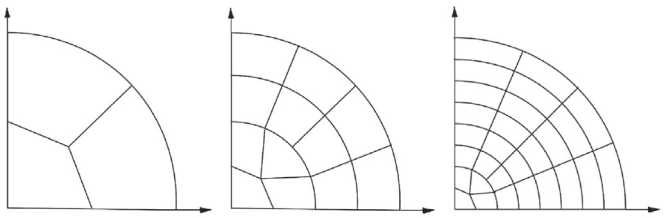

Fig. 8. The finite element discretisations ($N = 3$, 12, 28) of the circular plate.

The results are summarized in Tables 2 and 3 for the present separated variable approach using isoparametric and CL8 approximations. For the small thickness $h = 0.1$, VS-LD4/ISO exhibits transverse shear locking for both boundary conditions and convergence is very slow while convergence velocity of the F.E based on CL8 approximation are not sensitive to thickness. The new approximation in the separated representation drives to a higher convergence velocity. In fact, a $N = 3$ and $N = 12$ mesh are sufficient to recover accurate results for SA-2 and ENC, respectively (error of about 1% or less).

6.3. The homogeneous tests

The present issue is focused on the convergence of displacement and stresses predicted by the proposed CL8 element for a plate bending problem. The benchmark problem is defined as follows:

geometry: square plate of length $a = 0.1$ and length-to-thickness ratios $S = \frac{a}{h} = 2$, 5, 10, 100;
boundary conditions: simply supported on all sides with a bi-sinusoidal transverse distributed load on the top surface

Table 2
Tranverse displacement for circular plate - $h = 1$.

N	VS-LD4/CL8	%	VS-LD4/ISO	%
ENC	3D ref. solution: 0.715E-09			
1	5.946E-10	16.8%	3.975E-10	44.4%
3	6.862E-10	4.0%	6.618E-10	7.4%
12	7.013E-10	1.9%	6.787E-10	5.1%
28	7.134E-10	0.2%	7.085E-10	0.9%
SA-2	3D ref. solution: 0.258E-8			
1	2.470E-09	4.3%	2.031E-09	21.3%
3	2.580E-09	0.0%	2.498E-09	3.2%
12	2.576E-09	0.1%	2.479E-09	3.9%
28	2.580E-09	0.0%	2.572E-09	0.3%

Table 3
Tranverse displacement for circular plate - $h = 0.1$.

N	VS-LD4/CL8	%	VS-LD4/ISO	%
ENC	3D ref. solution: 0.61147e-6			
1	6.307E-08	89.7%	6.595E-09	98.9%
3	5.647E-07	7.6%	3.209E-07	47.5%
12	6.010E-07	1.7%	3.849E-07	37.1%
28	6.060E-07	0.9%	5.454E-07	10.8%
SA-2	3D ref. solution: 0.24895E-5			
1	2.237E-06	10.2%	2.977E-07	88.0%
3	2.488E-06	0.1%	1.472E-06	40.9%
12	2.488E-06	0.0%	1.625E-06	34.7%
28	2.485E-06	0.2%	2.251E-06	9.6%

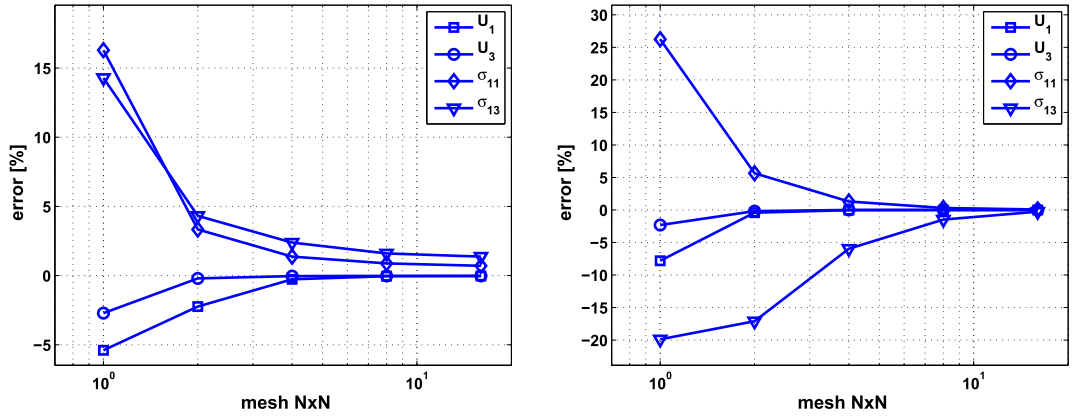

Fig. 9. Isotropic square plate under mechanical load; convergence for displacement and stresses for $S = 2$ (left) and $S = 100$ (right).

$p_3(x, y, z = \frac{h}{2}) = p_0 \ \sin\frac{\pi x}{a} \ \sin\frac{\pi y}{b}$
materials: isotropic material with $E = 73$ GPa and $\nu = 0.34$
mesh: $N = 1, 2, 4, 8, 16$ is used for the quarter of the plate
results: displacements and stresses are made non-dimensional according to

$$\overline{U}_1 = U_1 \ \frac{E\,h^2}{p_0\,a^3}; \ \ \overline{U}_3 = U_3 \ \frac{100\,E\,h^3}{p_0\,a^4}; \ \ \overline{\sigma}_{11} = \sigma_{11} \ \frac{1}{p_0\,S^2}; \ \ \overline{\sigma}_{i3} = \sigma_{i3} \ \frac{1}{p_0\,S}$$

location: displacements and stresses are calculated at the following points

$$U_1 \ : (0, b/2, -h/2); \ \ U_3, \sigma_{11}, \sigma_{33} \ : (a/2, b/2, h/2); \ \ \sigma_{13} \ : (0, b/2, 0)$$

reference values: the three dimensional exact elasticity results are obtained as in Ref. [52].

The convergence behavior for displacements and stresses of the CL8 element is shown in Fig. 9, where both very thick ($S = 2$) and thin ($S = 100$) plates are considered. The FE error is defined with respect to the three dimensional exact solution from Ref. [52]. The convergence rate is very satisfactory regardless of the length-to-thickness ratio. As expected, the convergence rate of the displacements is higher, and a $N = 4$ mesh is suitable. On the contrary, a more refined mesh is required for the transverse shear stress and a $N = 8$ drives to an error rate of about 1%. Nevertheless, the performance of this FE is rather very good.

6.4. *Laminated composite test: three-layered plates* ($0°/90°/0°$)

As the present approach based on the separated representation is particularly suitable for composite structures, a simply-supported laminated plate submitted to a bi-sinusoidal pressure is considered. The test aims at showing the performance of the proposed correction for such structures. It is described below:

Table 4
Convergence study - three layers ($0°/90°/0°$) – $S = 100$.

model	N	$\bar{u}(h/2)$	$\bar{v}(-h/2)$	$\bar{w}(0)$	$\bar{\sigma}_{11}(h/2)$	$\bar{\sigma}_{22}(-h/6)$	$\bar{\sigma}_{12}(h/2)$	$\bar{\sigma}_{13}(0)$	$\bar{\sigma}_{23}(0)$
VS-LD4/CL8	2	0.29%	0.58%	0.18%	5.18%	5.40%	4.84%	1.60%	5.10%
	4	0.00%	0.02%	0.01%	1.32%	1.29%	1.24%	0.72%	2.21%
	8	0.01%	0.00%	0.00%	0.33%	0.32%	0.31%	0.15%	0.52%
VS-LD4/ISO	2	1.18%	0.37%	4.83%	6.09%	8.79%	4.98%	146.32%	642.09%
	4	0.04%	0.60%	0.48%	0.06%	1.28%	1.59%	60.22%	210.62%
	8	0.01%	0.13%	0.04%	0.20%	0.07%	0.38%	19.76%	122.48%

Table 5
Three layers ($0°/90°/0°$) – $N = 8$.

S	model	$\bar{u}(h/2)$	$\bar{v}(-h/2)$	$\bar{w}(0)$	$\bar{\sigma}_{11}(h/2)$	$\bar{\sigma}_{22}(-h/6)$	$\bar{\sigma}_{12}(h/2)$	$\bar{\sigma}_{13}(0)$	$\bar{\sigma}_{23}(0)$
4	VS-LD4/CL8	−0.0097	0.0228	2.0059	0.8037	−0.5581	−0.0512	0.2568	0.2187
	error	0.04%	0.00%	0.00%	0.36%	0.33%	0.29%	0.34%	0.68%
	VS-LD4/ISO	−0.0097	0.0228	2.0059	0.8034	−0.5581	−0.0512	0.2566	0.2196
	error	0.00%	0.00%	0.00%	0.32%	0.32%	0.32%	0.26%	1.11%
	exact	−0.0097	0.0228	2.0059	0.8008	−0.5563	−0.0511	0.2559	0.2172
10	VS-LD4/CL8	−0.0074	0.0111	0.7530	0.5928	−0.2892	−0.0289	0.3584	0.1232
	error	0.05%	0.01%	0.00%	0.37%	0.33%	0.28%	0.31%	0.33%
	VS-LD4/ISO	−0.0074	0.0111	0.7530	0.5925	−0.2891	−0.0289	0.3588	0.1266
	error	0.00%	0.00%	0.00%	0.32%	0.32%	0.32%	0.43%	3.13%
	exact	−0.0074	0.0111	0.7530	0.5906	−0.2882	−0.0288	0.3573	0.1228
100	VS-LD4/CL8	−0.0068	0.0068	0.4347	0.5410	−0.1814	−0.0214	0.3941	0.0824
	error	0.01%	0.00%	0.00%	0.33%	0.32%	0.31%	0.15%	0.52%
	VS-LD4/ISO	−0.0068	0.0068	0.4345	0.5403	−0.1807	−0.0214	0.4727	0.1843
	error	0.01%	0.13%	0.04%	0.20%	0.07%	0.38%	19.76%	122.48%
	exact	−0.0068	0.0068	0.4347	0.5393	−0.1808	−0.0214	0.3947	0.0828

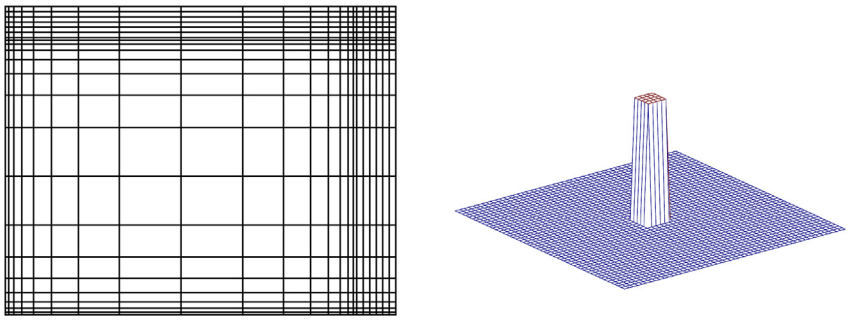

Fig. 10. Mesh $N = 22$ sr(18) (left) - localized pressure (right).

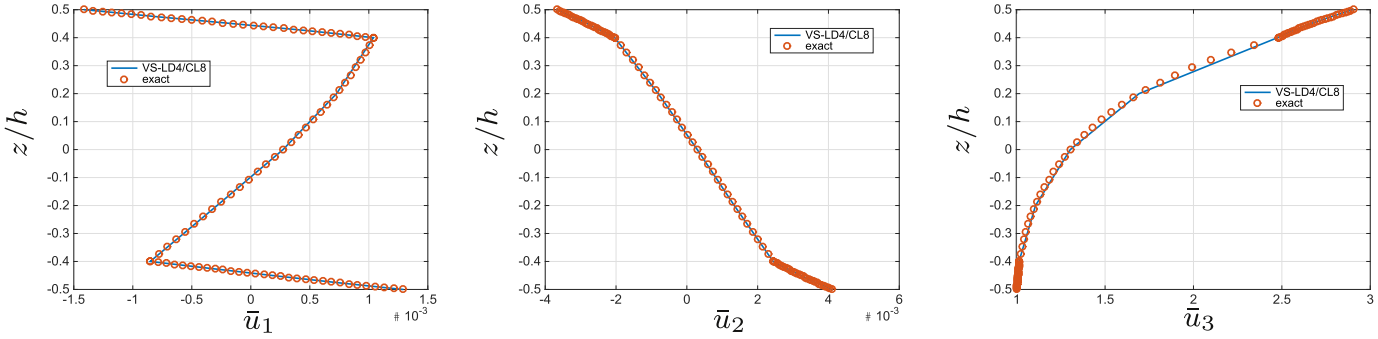

Fig. 11. Distribution of $\bar{u}_1$ (left), $\bar{u}_2$ (middle) and $\bar{u}_3$ (right) along the thickness - S = 2 - sandwich.

geometry: rectangular composite cross-ply plate (0°/90°/0°) with $b = a$. All layers have the same thickness. $S = \frac{a}{h} \in \{4, 10, 100\}$
boundary conditions: simply-supported plate on all sides subjected to a bi-sinusoidal pressure $q(x, y) = q_0 \sin\frac{\pi x}{a} \sin\frac{\pi y}{b}$

material properties: $E_L = 25$ GPa, $E_T = 1$ GPa, $G_{LT} = 0.2$ GPa, $G_{TT} = 0.5$ GPa, $\nu_{LT} = \nu_{TT} = 0.25$

where L refers to the fiber direction, T refers to the transverse direction.
mesh: $N = 8$, only one quarter of the plate is meshed.
results: The results are made nondimensional using:

$$\overline{u} = u_1(0, b/2, z)\frac{E_T}{hq_0S^3}, \quad \overline{v} = u_2(a/2, 0, z)\frac{E_T}{hq_0S^3},$$

$$\overline{w} = u_3(a/2, b/2, z)\frac{100E_T}{S^4hq_0}$$

$$\overline{\sigma}_{\alpha\alpha} = \frac{\sigma_{\alpha\alpha}(a/2, b/2, z)}{q_0S^2}, \quad \overline{\sigma}_{12} = \frac{\sigma_{12}(0, 0, z)}{q_0S^2}$$

$$\overline{\sigma}_{13} = \frac{\sigma_{13}(0, b/2, z)}{q_0S}, \quad \overline{\sigma}_{23} = \frac{\sigma_{23}(a/2, 0, z)}{q_0S}$$

reference values: the three-dimensional exact elasticity results are obtained as in Ref. [53].

First, a convergence study is carried out to compare the CL8 and ISO approach. The results are given in Table 4 for a thin plate. For the CL8 approximation, the results show that a $N = 8$ mesh provides converged FEM results (displacements and stresses) with respect to the exact solution, thus confirming the performances for the isotropic plate. For the ISO approach, it should be noted that the convergence of the transverse shear stresses is very low, while those of the displacements are good. The error rate is more than 100% for a N = 8

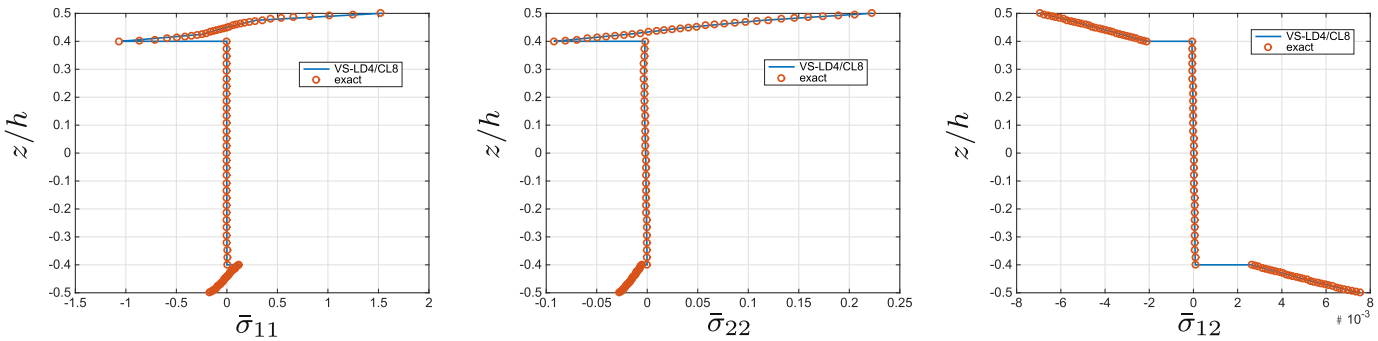

Fig. 12. Distribution of $\overline{\sigma}_{11}$ (left), $\overline{\sigma}_{22}$ (middle) and $\overline{\sigma}_{12}$ (right) along the thickness - S = 2 - sandwich.

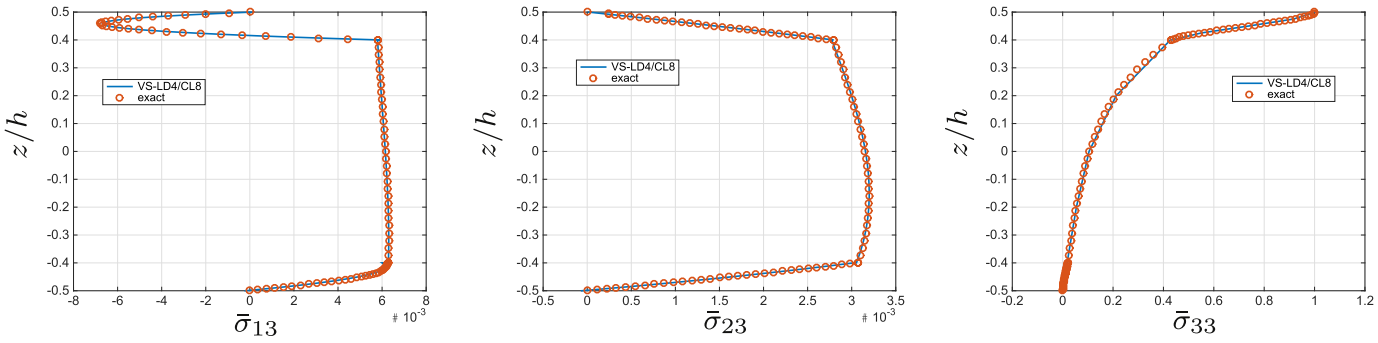

Fig. 13. Distribution of $\overline{\sigma}_{13}$ (left), $\overline{\sigma}_{23}$ (middle) and $\overline{\sigma}_{33}$(right) along the thickness - S = 2 - sandwich.

Table 6
Sandwich plate - localized pressure - $N = 22$ sr(18).

S	model	$\bar{u}(h/2)$	$\overline{v}(-h/2)$	$\overline{w}(0)$	$\overline{\sigma}_{11}(h/2)$	$\overline{\sigma}_{22}(h/2)$	$\overline{\sigma}_{12}(h/2)$	$\overline{\sigma}_{13}(0)$	$\overline{\sigma}_{13}$ max	$\overline{\sigma}_{23}(0)$
2	VS-LD4/CL8	−0.0014	0.0041	1.3033	1.5283	0.2219	−0.0069	0.0061	−0.0067	0.0032
	error	0.46%	0.21%	0.15%	0.67%	0.01%	0.07%	0.18%	1.34%	0.27%
	exact	−0.0014	0.0041	1.3052	1.5181	0.2219	−0.0069	0.0062	−0.0068	0.0031
4	VS-LD4/CL8	−0.0007	0.0026	0.4857	0.5670	0.0745	−0.0045	0.0076	0.0076	0.0017
	error	0.27%	0.00%	0.02%	0.83%	0.09%	0.11%	0.04%	0.04%	0.24%
	exact	−0.0007	0.0026	0.4858	0.5624	0.0746	−0.0045	0.0076	0.0076	0.0017
10	VS-LD4/CL8	−0.0006	0.0009	0.1362	0.1699	0.0235	−0.0020	0.0097	0.0097	−0.0004
	error	0.40%	1.09%	0.32%	0.15%	0.02%	0.90%	0.69%	0.69%	1.38%
	exact	−0.0006	0.0009	0.1366	0.1701	0.0235	−0.0020	0.0098	0.0098	−0.0004
40	VS-LD4/CL8	−0.0006	0.0003	0.0520	0.0902	0.0129	−0.0010	0.0103	0.0103	−0.0007
	error	0.14%	0.75%	0.12%	0.02%	0.38%	0.58%	0.02%	0.02%	1.68%
	exact	−0.0006	0.0003	0.0521	0.0902	0.0128	−0.0010	0.0103	0.0103	−0.0007

mesh. This test illustrates the efficiency of the proposed correction on all results. This error rate becomes less than 1% using the new approximation.

Based on the previous study, a $N = 8$ mesh is used for the analysis of the three-layer case with different slenderness ratios, $S = 4$, 10, 100. The results using both the ISO and CL8 approaches are summarized in Table 5. The accuracy of the results is very satisfactory for both displacements and stresses, excepted for the transverse shear stresses for moderately thick to thin plates (from 3.13% to 122% with a ISO approach). To overcome this drawback, the new CL8 approximation is used advantageously. The error rate decreases significantly (less than 0.52%).

6.5. *Sandwich plate under localized pressure*

In this section, the analysis of a sandwich plate with local effects is carried out for a wide range of slenderness ratios. The test is detailed below:

geometry: square sandwich plate with length-to-thickness ratios $S \in \{2, 4, 10, 100, 1000\}$. The thickness of each face sheet is $\frac{h}{10}$.

boundary conditions: simply-supported plate subjected to a localized pressure $q(x, y) = q_0$ applied on a square area with a size of $a/10 \times a/10$ at the plate center (see Fig. 10 right).

material properties: The material of the face sheet is the same as in Section 6.4.

The core material is transversely isotropic with respect to z and is characterized by:

$$E_{xx} = E_{yy} = 0.04 \text{ GPa}, \quad E_{zz} = 0.5 \text{ GPa}, \quad G_{xz} = G_{yz} = 0.06 \text{ GPa},$$
$$G_{xy} = 0.016 \text{ GPa}, \quad \nu_{xz} = \nu_{yz} = 0.02, \quad \nu_{xy} = 0.25$$

mesh: $N = 22$ with a space ratio of 18, denoted sr(18) is used for the quarter of the plate (see Fig. 10 left). 6×6 elements are used for the pressure area.

results: displacements and stresses are made non-dimensional as in Section 6.4.

reference values are obtained with 450 terms in the Fourier series ([53]). The applied pressure is shown in Fig. 10 right.

Table 7
Sandwich plate - localized pressure - $N = 22$ sr(18).

S	model	$\bar{u}(h/2)$	$\overline{v}(-h/2)$	$\overline{w}(0)$	$\overline{\sigma}_{11}(h/2)$	$\overline{\sigma}_{22}(h/2)$	$\overline{\sigma}_{12}(h/2)$	$\overline{\sigma}_{13}(0)$	$\overline{\sigma}_{23}(0)$
	VS-LD4/CL8	−6.35e-04	2.83e-04	4.66e-02	8.76e-02	1.12e-02	−8.84e-04	1.02e-02	−7.34e-04
		0.07%	0.10%	0.05%	0.05%	0.11%	0.12%	0.47%	0.99%
100	VS-LD4/ISO	−6.35e-04	2.84e-04	4.65e-02	8.77e-02	1.12e-02	−8.86e-04	1.01e-02	−7.51e-04
		0.12%	0.43%	0.13%	0.03%	0.00%	0.41%	0.07%	1.38%
	exact	−6.35e-04	2.83e-04	4.66e-02	8.77e-02	1.12e-02	−8.82e-04	1.01e-02	−7.41e-04
	VS-LD4/CL8	−6.35e-04	2.75e-04	4.55e-02	8.75e-02	1.08e-02	−8.65e-04	1.00e-02	−7.45e-04
		0.15%	0.30%	0.14%	0.04%	0.01%	0.31%	0.13%	0.25%
1000	VS-LD4/ISO	−6.35e-04	2.75e-04	4.53e-02	8.74e-02	1.08e-02	−8.65e-04	1.07e-02	−2.43e-03
		0.17%	0.37%	0.40%	0.15%	0.10%	0.36%	6.52%	226.86%
	exact	−6.36e-04	2.76e-04	4.55e-02	8.75e-02	1.08e-02	−8.68e-04	1.01e-02	−7.43e-04

The number of couples built by the present approach VS-LD4/CL8 varies from five for S = 1000 to twenty-one for $S = 2$. The number of couples increases with the thickness of the structure. For the very thick case ($S = 2$), the distributions of the displacements and stresses through the thickness are presented in Figs. 11–13. It can be inferred from these figures that the present approach is in excellent agreement with the reference solution despite the complexity of the variations of these quantities. For the in-plane displacement, a zig-zag effect occurs and the variation through the core is not strictly linear. We also notice that the in-plane stresses $\sigma_{\alpha\alpha}$, $\alpha = 1, 2$ are influenced by the localized pressure, especially in the upper layer. The evolution of σ_{11} through the thickness becomes highly non-linear in this layer. Moreover, a strong non-symmetric distribution appears. This specific behavior is well-captured. For the transverse shear and normal stresses, both the upper and lower conditions and the interface continuity ones are satisfied. The particular behavior of σ_{13} in Fig. 13 (left) is due to the slenderness ratio and the localized load. The maximum value is located in the upper layer where high variations occur. Only layerwise-type approaches have the capability to represent such phenomena.

In Table 6, it is confirmed that the results perform very well with respect to the reference solution. The maximum error rate remains less than 1.6%. Again, a particular attention is paid on the results for very thin case ($S = 100, 1000$), see Table 7. The limitation of the isoparametric approach is clearly shown. While the quality of the ISO results is affected by the slenderness ratio, the accuracy of the transverse shear stresses can be improved by the CL8 approximation without any mesh refinement.

7. Conclusion

In this paper, an approach based on the separation of variables for the modeling of composite/sandwich plates in conjunction with a new FE approximation of only the constant part of the transverse shear strain is proposed. It requires to extend the so-called CL8 FE in this particular framework. Thus, a locking-free approach is derived. The robustness and accuracy of the proposed method is assessed by referring to some recommended tests, namely, (i) convergence behavior for thin and thick plates under various boundary and loading conditions, (ii) test cases involving distorted meshes. The numerical results confirm the superiority of the proposed FE in comparison to classical isoparametric approaches with full integrations: it is free of transverse shear locking and is less sensitive to distorted element shapes, showing a high convergence rate for both displacements and stresses. The model performs also very well for both laminated composite and sandwich plates under global or localized loads. Moreover, the excellent performance of this new approach is shown for very thick to very thin structures. Thus, this new FE has proven and enhanced robustness. It can be hence used to model a broad class of problems.

Based on these convincing results, the method could be extended to shell structures.

Appendix A. Finite element approximations

Appendix A.1 The eight node interpolation

The interpolation functions on the elementary domain are defined as follow:

$$\forall(\xi,\eta)\in[-1,1]^2,\quad p(\xi,\eta)=\sum_{i=1}^{8} Nq_i(\xi,\eta)\,p_i \quad \text{with}$$

$$Nq_1(\xi,\eta)=-\frac{1}{4}(1-\xi)(1-\eta)(1+\xi+\eta) \qquad Nq_2(\xi,\eta)=-\frac{1}{4}(1+\xi)(1-\eta)(1-\xi+\eta)$$

$$Nq_3(\xi,\eta)=-\frac{1}{4}(1+\xi)(1+\eta)(1-\xi-\eta) \qquad Nq_4(\xi,\eta)=-\frac{1}{4}(1-\xi)(1+\eta)(1+\xi-\eta)$$

$$Nq_5(\xi,\eta)=\frac{1}{2}(1-\xi^2)(1-\eta) \qquad Nq_6(\xi,\eta)=\frac{1}{2}(1+\xi)(1-\eta^2)$$

$$Nq_7(\xi,\eta)=\frac{1}{2}(1-\xi^2)(1+\eta) \qquad Nq_8(\xi,\eta)=\frac{1}{2}(1-\xi)(1-\eta^2)$$

References

[1] J.N. Reddy, Mechanics of Laminated Composite Plates and Shells – Theory and Analysis, CRC Press Inc., 2004.
[2] Y. Tanigawa, H. Murakami, Y. Ootao, Transient thermal stress analysis of a laminated composite beam, J. Therm. Stress. 12 (1989) 25–39.
[3] P.C. Yang, C.H. Norris, Y. Stavsky, Elastic wave propagation in heterogeneous plates, Int. J. Solids Struct. 2 (1966) 665–684.
[4] K.H. Lo, R.M. Christensen, F.M. Wu, A higher-order theory of plate deformation. part ii: laminated plates, J. Appl. Mech. ASME 44 (1977) 669–676.
[5] E. Carrera, A priori vs. a posteriori evaluation of transverse stresses in multilayered orthotropic plates, Compos. Struct. 48 (4) (2000) 245–260.
[6] T. Kant, K. Swaminathan, Analytical solutions for the static analysis of laminated composite and sandwich plates based on a higher order refined theory, Compos. Struct. 56 (2002) 329–344.
[7] J.N. Reddy, A simple higher-order theory for laminated composite plates, J. Appl. Mech. ASME 51 (4) (1984) 745–752.
[8] J.N. Reddy, An evaluation of equivalent-single-layer and layerwise theories of composite laminates, Compos. Struct. 25 (1993) 21–35.
[9] M. Touratier, An efficient standard plate theory, Int. J. Eng. Sci. 29 (1991) 901–916.
[10] N.J. Pagano, Exact solutions for composite laminates in cylindrical bending, J. Comp. Mater. 3 (1969) 398–411.
[11] J.N. Reddy, On refined computational models of composite laminates, Int. J. Numer. Methods Eng. 27 (1989) 361–382.
[12] D.H. Robbins, J.N. Reddy, Modeling of thick composites using a layerwise laminate theory, Int. J. Numer. Methods Eng. 36 (1993) 655–677.
[13] E. Carrera, Evaluation of layerwise mixed theories for laminated plates analysis, AIAA J. 36 (5) (1998) 830–839.
[14] E. Carrera, A study of transverse normal stress effect on vibration of multilayered plates and shells, J. Sound Vib. 225 (1999) 803–829.
[15] U. Icardi, Higher-order zig-zag model for analysis of thick composite beams with inclusion of transverse normal stress and sublaminates approximations, Compos. Part B Eng. J. 32 (2001) 343–354.
[16] R.P. Shimpi, A.V. Ainapure, A beam finite element based on layerwise trigonometric shear deformation theory, Compos. Struct. 53 (2001) 153–162.
[17] A.J.M. Ferreira, Analysis of composite plates using a layerwise shear deformation theory and multiquadrics discretization, Mech. Adv. Mater. Struct. 12 (2005) 99–112.
[18] E. Carrera, L. Demasi, Classical and advanced multilayered plate elements based upon pvd and rmvt. part 1: derivation of finite element matrices, Int. J. Numer. Methods Eng. 55 (2002) 191–231.
[19] C.-Y. Lee, D. Liu, X. Lu, Static and vibration analysis of laminated composite beams with an interlaminar shear stress continuity theory, Int. J. Numer. Methods Eng. 33 (1992) 409–424.
[20] M. Di Sciuva, U. Icardi, Numerical assessment of the core deformability effect on the behavior of sandwich beams, Compos. Struct. 52 (2001) 41–53.

[21] S. Kapuria, P.C. Dumir, A. Ahmed, An efficient higher order zigzag theory for composite and sandwich beams subjected to thermal loading, Int. J. Solids Struct. 40 (2003) 6613–6631.
[22] P. Vidal, O. Polit, A refined sinus plate finite element for laminated and sandwich structures under mechanical and thermomechanical loads, Comput. Methods Appl. Mech. Eng. 253 (2013) 396–412.
[23] A.K. Noor, W.S. Burton, Assessment of computational models for multilayered composite shells, Appl. Mech. Rev. 43 (4) (1990) 67–97.
[24] J.N. Reddy, Mechanics of Laminated Composite Plates - Theory and Analysis, CRC Press, Boca Raton, FL, 1997.
[25] E. Carrera, Theories and finite elements for multilayered, anisotropic, composite plates and shells, Arch. Comput. Methods Eng. 9 (2002) 87–140.
[26] E. Carrera, Historical review of zig-zag theories for multilayered plates and shells, Appl. Mech. Rev. 56 (3) (2003) 287–308.
[27] Y.X. Zhang, C.H. Yang, Recent developments in finite elements analysis for laminated composite plates, Compos. Struct. 88 (2009) 147–157.
[28] R.H. MacNeal, Perspective on finite elements for shell analysis, Finite Elem. Anal. Des. 30 (1998) 175–186.
[29] T.H.H. Pian, K. Sumihara, State-of-the-art development of hybrid/mixed finite element method, Finite Elem. Anal. Des. 21 (1995) 5–20.
[30] T. Belytschko, W.K. Liu, B. Moran, Nonlinear Finite Elements for Continua and Structures, second ed., John Wiley & Sons, 2000.
[31] T.J.R. Hughes, The Finite Element Method, Prentice Hall, Englewood Cliffs, New Jersey, 1987.
[32] T.J.R. Hughes, T.E. Tezduyar, Finite elements based upon mindlin plate theory with particular reference to the four-node bilinear isoparametric element, J. Appl. Mech. ASME 48 (1981) 587–596.
[33] R.H. MacNeal, Derivation of element stiffness matrices by assumed strain distributions, Nucl. Eng. Des. 70 (1982) 3–12.
[34] K.C. Park, E. Pramono, G.M. Stanley, H.A. Cabiness, The ans shell elements : earlier and recent improvements, in: Noor (Ed.), Analytical and Computational Models of Shells, vol. 3, 1989, pp. 359–382.
[35] K.J. Bathe, E.N. Dvorkin, A four-node plate bending element based on mindlin-reissner plate theory and a mixed interpolation, Int. J. Numer. Methods Eng. 22 (1985) 367–383.
[36] B.R. Somashekar, G. Prathap, C.R. Babu, A field consistent four-node laminated anisotropic plate/shell element, Comput. Struct. 25 (1987) 345–353.
[37] J.-L. Batoz, P. Lardeur, A discrete shear triangular nine d.o.f. element for the analysis of thick to very thin plates, Int. J. Numer. Methods Eng. 28 (1989) 533–560.
[38] K.U. Bletzinger, M. Bischoff, E. Ramm, A unified approach for shear-locking-free triangular and rectangular shell finite elements, Comput. Struct. 75 (2000) 321–334.
[39] A. Ammar, B. Mokdada, F. Chinesta, R. Keunings, A new family of solvers for some classes of multidimensional partial differential equations encountered in kinetic theory modeling of complex fluids, J. Non-Newt. Fluid Mech. 139 (2006) 153–176.
[40] M. Savoia, J.N. Reddy, A variational approach to three-dimensional elasticity solutions of laminated composite plates, J. Appl. Mech. ASME 59 (1992) 166–175.
[41] B. Bognet, F. Bordeu, F. Chinesta, A. Leygue, A. Poitou, Advanced simulation of models defined in plate geometries: 3D solutions with 2D computational complexity, Comput. Methods Appl. Mech. Eng. 201–204 (2012) 1–12, https://doi.org/10.1016/j.cma.2011.08.025.
[42] P. Vidal, L. Gallimard, O. Polit, Assessment of a composite beam finite element based on the proper generalized decomposition, Compos. Struct. 94 (5) (2012) 1900–1910, https://doi.org/10.1016/j.compstruct.2011.12.016.
[43] P. Vidal, L. Gallimard, O. Polit, Proper generalized decomposition and layer-wise approach for the modeling of composite plate structures, Int. J. Solids Struct. 50 (14–15) (2013) 2239–2250, https://doi.org/10.1016/j.ijsolstr.2013.03.034.
[44] P. Vidal, L. Gallimard, O. Polit, Assessment of variable separation for finite element modeling of free edge effect for composite plates, Compos. Struct. 123 (-) (2015) 19–29, https://doi.org/10.1016/j.compstruct.2014.11.068.
[45] G. Giunta, S. Belouattar, O. Polit, L. Gallimard, P. Vidal, M. D'Ottavio, Hierarchical beam finite elements based upon a variables separation method, Int. J. Appl. Mech. 8 (2) (2016) 1650026–1650035, https://doi.org/10.1142/S1758825116500265.
[46] O. Polit, M. Touratier, P. Lory, A new eight-node quadrilateral shear-bending plate finite element, Int. J. Numer. Methods Eng. 37 (1994) 387–411.
[47] O. Polit, P. Vidal, M. D'Ottavio, Robust C^0 high-order plate finite element for thin to very thick structures: mechanical and thermo-mechanical analysis, Int. J. Numer. Methods Eng. 40 (2012) 429–451, https://doi.org/10.1002/nme.3328.
[48] T.H.C. Le, M. D'Ottavio, P. Vidal, O. Polit, A new robust quadrilateral four-node variable kinematics plate element for composite structures, Finite Elem. Anal. Des. 133 (2017) 10–24, https://doi.org/10.1016/j.finel.2017.05.002.
[49] O. Polit, M. Touratier, P. Lory, A new eight-node quadrilateral shear-bending plate finite element, Int. J. Numer. Methods Eng. 37 (1994) 387–411.
[50] M. Ganapathi, O. Polit, M. Touratier, A c^0 eight-node membrane-shear-bending element for geometrically non-linear (static and dynamic) analysis of laminates, Int. J. Numer. Methods Eng. 39 (1996) 3453–3474.
[51] S. Klinkel, F. Gruttmann, W. Wagner, A continuum based three dimensional shell element for laminated structures, Comput. Struct. 71 (1999) 43–62.
[52] L. Demasi, ∞^3 plate theories for thick and thin plates: the generalized unified formulation, Compos. Struct. 84 (2008) 256–270.
[53] N.J. Pagano, Exact solutions for rectangular bidirectional composites and sandwich plates, J. Comp. Mater. 4 (1970) 20–34.